Isomeric and concentration effects of C_4-cosurfactants on four-component microemulsions investigated by neutron spin-echo and small-angle scattering

2006 J. Phys.: Condens. Matter 18 S2451

(http://iopscience.iop.org/0953-8984/18/36/S17)

INSTITUTE OF PHYSICS PUBLISHING JOURNAL OF PHYSICS: CONDENSED MATTER

J. Phys.: Condens. Matter **18** (2006) S2451–S2466 doi:10.1088/0953-8984/18/36/S17

Isomeric and concentration effects of C_4-cosurfactants on four-component microemulsions investigated by neutron spin-echo and small-angle scattering

E Zambrano[1], M Kotlarchyk[2,6], A Langner[3] and A Faraone[4,5]

[1] Center for Materials Science and Engineering, Rochester Institute of Technology, Rochester, NY 14623, USA
[2] Department of Physics, Rochester Institute of Technology, Rochester, NY 14623, USA
[3] Department of Chemistry, Rochester Institute of Technology, Rochester, NY 14623, USA
[4] NIST Center for Neutron Research, Gaithersburg, MD 20899, USA
[5] Department of Material Science and Engineering, University of Maryland, College Park, MD 20742, USA

E-mail: mnksps@rit.edu (M Kotlarchyk)

Received 31 January 2006, in final form 21 April 2006
Published 24 August 2006
Online at stacks.iop.org/JPhysCM/18/S2451

Abstract

Neutron spin-echo spectroscopy and small-angle scattering measurements were performed to determine how the isomeric structure and concentration of C_4-cosurfactants (i.e. butyl alcohols) influence structure and dynamics in four-component water-in-oil microemulsions. The system investigated was AOT/butanol/water/n-octane at room temperature (AOT denotes sodium di-2-ethyl hexylsulfosuccinate), deuterated to achieve contrast of the surfactant/cosurfactant film. At a fixed volume fraction of 0.06 and a fixed molar ratio of [water]/[AOT] = 20, we studied the effects of increasing the molar ratio of [butanol]/[AOT] from 0 to 30. Data from samples containing the cosurfactant n-butyl alcohol were compared with samples prepared with tert-butyl alcohol and, in a few cases, sec-butyl alcohol. Data were analysed using a core–shell model for polydisperse spherical droplets, allowing for the presence of shape fluctuations. It was found that all structural isomers of the cosurfactant led to a similar decrease in droplet size with increasing alcohol content. In all cases, droplet size and shape fluctuations were observed to increase with alcohol content; however, the effect was most pronounced for size fluctuations (i.e. polydispersity) in the presence of tert-butanol. The data indicates that tert-butanol has a higher degree of penetration into the water core, leading to a reduced influence on the effective area per surfactant head group on the droplet surface. There is also evidence that an increased droplet–droplet attraction upon adding tert-butanol drives phase separation in the system.

[6] Author to whom any correspondence should be addressed.

1. Introduction

The structure and dynamics of water-in-oil droplets in single-phase ternary microemulsions are well understood [1, 2]. In the system containing the surfactant AOT (sodium di-2-ethylhexylsulfosuccinate), the mean droplet core radius (≈50 Å) increases linearly with the water-to-surfactant molar ratio, W, and maintains this size independently of oil dilution, up to very high values of the total droplet volume fraction ϕ [3, 4]. It has been shown that these droplets experience significant dynamical size fluctuations (i.e. polydispersities of 20–30%), as well as peanut-like shape deformations [5]. The size, shape, and fluctuations of the droplet interface are governed by the form of the Helmholtz free energy which, to lowest order in the interface thickness, is a sum of the Helfrich elastic curvature energy and the entropy of mixing. Expanding the shape of the droplet surface in terms of spherical harmonics allows for the identification of the various shape fluctuation modes. The length scales associated with the microemulsion droplet structure and the time scales of the shape fluctuations are ideally suited for investigation by small-angle neutron scattering (SANS) and neutron spin-echo (NSE) spectroscopy [6]. Such studies have been performed by Farago *et al* [7, 8] and Huang *et al* [9] on the three-component AOT/water/n-decane system at room temperature ($8 < W < 40, \phi \approx 0.05$), resulting in values for κ, the interface bending elastic modulus, in the neighbourhood of $3.5k_BT$, and typical $l = 2$ (peanut-like) fluctuation amplitudes (root mean square) of about 10–20% of the radius. Kawabata *et al* [10] has reported values corresponding to a much more flexible droplet interface ($\kappa \approx 0.3k_BT$, amplitude ≈80%) for the latter room-temperature system ($W = 18.4$, $\phi = 0.10$), attributing the discrepancy in results, at least in part, to fitting their NSE data without the benefit of corroborating dynamic light scattering measurements [11, 12].

The influence on the size and shape fluctuations of the interface produced by adding n-butyl alcohol as a cosurfactant in the AOT/water/n-decane system has been investigated by Farago *et al* [13]. The study was performed at a fixed droplet volume-fraction of 6% and for values of the butanol-to-AOT molar ratio, α, in the range 0 to 30. The value of W was adjusted ($24 < W < 37$) in order to maintain a droplet core radius of ≈35 Å. The results show that the addition of the alcohol leads to a systematic increase in fluctuations of the interface and a corresponding decrease in the elastic bending modulus.

The goal of the present study is to use SANS and NSE to investigate how various structural isomers of butyl alcohol affect structure and fluctuations in the AOT system at room temperature. The effect of three butyl alcohols is explored: n-butyl alcohol (n-BA), sec-butyl alcohol (s-BA), and tert-butyl alcohol (t-BA). The structure of each alcohol is shown in figure 1. The water and oil components of the microemulsions are fully deuterated in order to achieve maximum shell contrast for neutron scattering. In our experiments, we systematically vary α, while maintaining $W = 20$ (hence, we expect droplet size to change) and $\phi = 0.06$. With n-decane as the oil, we have observed that the room-temperature system containing tert-butanol phase separates at low values of α. Consequently, deuterated n-octane is chosen as the oil component in our study since, in that case, no phase separation occurs over an extended range of α for $W = 20$.

Fluorescence measurements performed in our laboratory provide firm evidence that the alcohol resides almost exclusively within the droplet structure, rather than the oil continuum. The signal from an N-piperdyl dansylamide fluorescence probe (with an excitation wavelength of 330 nm), dissolved in pure oil, exhibits an easily observable intensity decrease and red-shift of the emission upon adding increasing amounts of butyl alcohol. When dissolved in a microemulsion, this probe partitions between the droplets and the hydrocarbon continuum. The component of the emission attributable to the droplet varies with alcohol content, whereas

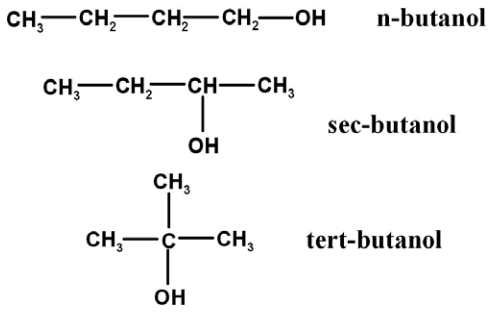

Figure 1. Three structural isomers of the butyl alcohol cosurfactant, $C_4H_{10}O$ (mol wt = 74.1 g mol^{-1}).

the hydrocarbon-based component is indistinguishable from that of the pure oil. Hence, we conclude that essentially no alcohol resides outside the droplets, and the total volume fraction, ϕ, is a sum of the water, surfactant, and alcohol volume fractions.

2. Experiments

2.1. Samples

AOT (mol wt 444.5 g mol^{-1}) was purchased from Fluka and was purified by a standard procedure [14]. Deuterated water (D_2O; 99.9 atom% D) and deuterated n-octane (C_8D_{18}; 99% atom% D) were obtained from J T Baker and Cambridge Isotope Laboratories, respectively. Butyl alcohols were supplied by Sigma-Aldrich Chemical Co. with >99.4% purity.

Microemulsions were prepared by starting with a three-component stock solution (no alcohol) with $W = 20.0$. For each sample, in order to produce the desired α-value, yet maintain the same volume fraction of $\phi = 0.06$, precisely calculated and measured volumes of the stock solution, deuterated octane, and the appropriate type of alcohol were combined. (Specific gravity values of 1.13, 0.815, 0.840, 0.838, and 0.825 were used for AOT, deuterated n-octane, n-BA, s-BA, and t-BA, respectively. The values for the alcohols were based on measured specific volumes in alcohol/water mixtures.) The scattering experiments took place within a week of sample preparation. Because almost a year elapsed between performing the SANS and NSE experiments, a separate batch of samples was prepared for the two types of measurements.

2.2. Small-angle neutron scattering measurements

SANS measurements were performed using the NG-3 30 m small-angle scattering instrument operated by the Center for High-Resolution Neutron Scattering at the NIST Center for Neutron Research (NCNR) in Gaithersburg, Maryland [15]. The neutron wavelength was set at $\lambda = 6$ Å with $\delta\lambda/\lambda = 0.147$. For each sample, data were collected at two sample-to-detector distances (1.33 and 12.00 m) in order to span a wide range of Q-values [$Q = (4\pi/\lambda)\sin(\theta/2)$, where θ is the scattering angle] from ≈0.04 to 0.4 inverse angstroms. Raw data was radially averaged and corrected for transmission and empty-cell scattering. Scattering from the pure solvent (deuterated octane) was subtracted from the data, along with a flat incoherent background, calculated on the basis of the amount of protonated hydrogen present in both the alcohol and surfactant components of the sample. All samples were contained in 1 mm path-length cells with quartz windows and held at a temperature of 23.0 ± 0.1 °C.

The final data sets were recorded on an absolute scale, i.e. as macroscopic cross-sections, and all fitting models applied to the data were computed on an absolute scale. Furthermore, all models were smeared to the resolution of the instrument. The SANS data reduction software developed at NCNR was used for elements of the data reduction and analysis [16].

2.3. Neutron spin-echo measurements

NSE measurements were carried out on the NG-5 neutron spin-echo spectrometer at the NCNR [17]. The wavelength was 8 Å with $\delta\lambda/\lambda \approx 0.20$. The Q-range accessed was ≈0.05 to 0.14 inverse angstroms and the Fourier time window covered the range from 0.10 to 35 ns. Quartz sample cells with path lengths of 1 or 2 mm were used. Data have been corrected for the scattering from the empty cell and the pure solvent, and the instrumental resolution has been divided out using data collected from a reference elastic sample.

Thus, the normalized intermediate scattering functions, $I(Q,t)/I(Q,0)$, were obtained [6]. The observed correlation functions were fitted to a single-exponential decay, which allows for the determination of a Q-dependent effective diffusion coefficient, D_{eff}:

$$\frac{I(Q,t)}{I(Q,0)} = \exp\left[-D_{\text{eff}}(Q)Q^2 t\right]. \tag{1}$$

Hellweg and Langevin [12] have described a more refined model based on a double-exponential decay. However, based on the quality of the single-exponential fits to our data, the incorporation of a second exponential seemed to be unwarranted.

The DAVE software package was used for elements of the data reduction and analysis [18].

3. Scattering models

3.1. Droplet models for SANS

3.1.1. Simple polydisperse core–shell. In this model, it is assumed that the droplet consists of a uniform spherical core of radius R_c coated by a uniform spherical shell of thickness δ. The scattering-length densities of the core and shell are ρ_c and ρ_s, respectively, and the surrounding background medium has a scattering-length density set equal to that of the deuterated oil, ρ_o. The absolute scattering intensity is given by

$$I(Q) = \frac{4\pi\phi}{3\left\langle (R_c+\delta)^3\right\rangle_{R_c}} \langle P(Q)\rangle_{R_c}, \tag{2}$$

where

$$P(Q) = \frac{1}{Q^2}\left\{\Delta\rho_1 R_c^2 j_1(QR_c) + \Delta\rho_2 (R_c+\delta)^2 j_1\left[Q(R_c+\delta)\right]\right\}^2. \tag{3}$$

$j_1(x)$ is the first-order spherical Bessel function, and we define $\Delta\rho_1 \equiv \rho_s - \rho_c$ and $\Delta\rho_2 \equiv \rho_o - \rho_s$. The brackets $\langle\,\rangle_{R_c}$ denote an average over a Schultz distribution [19, 20] of core sizes characterized by a mean radius $\bar{R}_c$ and a polydispersity index $p \equiv \sigma_{R_c}/\bar{R}_c$. This polydispersity is, in actuality, a measure of the dynamical size fluctuations of the droplets [21]. Data is fitted with the five adjustable parameters $\bar{R}_c$, p, δ, ρ_c, and ρ_s, as well as a constant background term associated with residual incoherent scattering (ρ_o is set to 6.42×10^{-6} Å^{-2}, the value for deuterated octane).

3.1.2. Fluctuating polydisperse core–shell. Here, we add in the possibility of droplet shape fluctuations to the previous model. Following the work of Farago *et al* [22], we write

$$I(Q) = \frac{4\pi\phi}{3\left\langle (R_c+\delta)^3\right\rangle_{R_c}} \left\langle P(Q) + P_s(Q) + P_d(Q)\right\rangle_{R_c}, \tag{4}$$

which includes a static correction

$$P_s(Q) = \Big\{\Delta\rho_1 R_c\left[2j_0(QR_c) - QR_c j_1(QR_c)\right] + \Delta\rho_2(R_c+\delta)[2j_0\left[Q(R_c+\delta)\right] - Q(R_c+\delta)j_1\left[Q(R_c+\delta)\right]]\Big\} \times \frac{1}{4\pi}\sqrt{P(Q)}\sum_{l=2}^{\infty}(2l+1)\left\langle |a_l|^2\right\rangle \tag{5}$$

and a dynamic correction

$$P_d(Q) = \frac{1}{4\pi}\sum_{l=2}^{\infty}(2l+1)\left\langle |a_l|^2\right\rangle\left\{\Delta\rho_1 R_c^2 j_l(QR_c) + \Delta\rho_2(R_c+\delta)^2 j_l\left[Q(R_c+\delta)\right]\right\}^2 \tag{6}$$

involving lth-order spherical Bessel functions. a_l is the amplitude of the shape fluctuation associated with spherical harmonic Y_{l0}. The shape-fluctuation corrections to the intensity are valid up to second-order in the fluctuation amplitudes, whereas the size polydispersity, which corresponds to $l = 0$, or size fluctuations, is calculated exactly.

We can also define dimensionless root-mean-square amplitudes as $|u_l|_{\rm rms} \equiv \langle |a_l|^2\rangle^{1/2}/\bar{R}_c$. These are constrained by the values of the bending elastic modulus, κ, and the size polydispersity, p, according to [22]

$$|u_l|_{\rm rms} = \left\{(l+2)(l-1)\left[l(l+1)\frac{\kappa}{k_B T} - \frac{1}{8\pi p^2}\right]\right\}^{-1/2}. \tag{7}$$

Consequently, only one additional fitting parameter, i.e. κ, needs to be added to those appearing in the simple polydisperse core–shell model.

We benchmarked the effect of removing high-l contributions to the computed scattering intensity. In agreement with other workers [13, 22], it was observed that only the $l = 2$ shape fluctuations are observable. The $l > 2$ contributions are found to be negligible, and hence are omitted from the fitting procedure.

3.2. Fluctuating droplet model for NSE

We assume that the Q-dependent effective diffusion coefficient extracted from the NSE normalized intermediate scattering function is a sum of two contributions, i.e.

$$D_{\rm eff}(Q) = D_{\rm tr} + D_{\rm def}(Q), \tag{8}$$

where $D_{\rm tr}$ is the $Q \to 0$ translational diffusion coefficient of the droplet and $D_{\rm def}$ is the contribution due to droplet shape deformations. The dominant contribution to $D_{\rm def}$ is the $l = 2$ fluctuation mode, and can be modelled by [23]

$$D_{\rm def}(Q) = \frac{5\lambda_2 f_2(QR_o)\,|u_2|^2_{\rm rms}}{Q^2\left\{4\pi\left[j_0(QR_o)\right]^2 + 5f_2(QR_o)\,|u_2|^2_{\rm rms}\right\}}, \tag{9}$$

with $f_2(x) = [4j_2(x) - xj_3(x)]^2$. Here, R_o is the mean droplet radius (approximating the shell as being very thin) and λ_2^{-1} is the relaxation time for the $l = 2$ deformation mode. Hence, the $D_{\rm eff}$ versus Q data sets are fitted using four adjustable parameters: $D_{\rm tr}$, R_o, λ_2, and $|u_2|_{\rm rms}$. When we compare results, it is assumed that the NSE parameter R_o corresponds to the SANS radius $\bar{R}_c + \delta/2$, i.e. the radius obtained by collapsing the shell about its centre. The

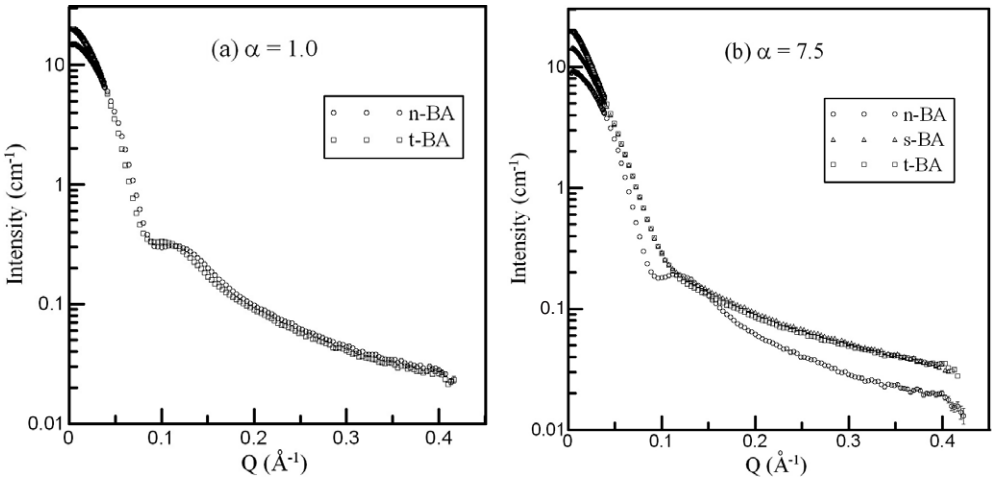

Figure 2. SANS data (with shell contrast) for microemulsions containing various butyl alcohol cosurfactants for two different values of the alcohol-to-AOT molar ratio, α.

bending modulus can be computed from the value of λ_2 and the value of the polydispersity, p, determined by SANS [24]:

$$\kappa = \frac{1}{48}\left(\frac{k_B T}{\pi p^2} + \lambda_2 \eta R_o \frac{23\eta' + 32\eta}{3\eta}\right). \tag{10}$$

$\eta = 0.56$ cp is the viscosity (at $T = 23\,^{\circ}$C) of the deuterated n-octane solvent and $\eta' = 1.14$ cp is the viscosity of the D_2O within the droplet.

4. Results and discussion

SANS data are shown in figures 2, 3, and 4. Figure 2 illustrates the effect of changing alcohol structure for two particular values of the alcohol content, α. At a relatively low alcohol-to-surfactant ratio ($\alpha = 1.0$), the data are quite similar, with the tert-butanol microemulsion exhibiting a peak shifted to slightly lower Q and with a slight degree of broadening. At much higher alcohol content ($\alpha = 7.5$), the n-butanol microemulsion still exhibits a peak, but the peak is absent from the sample containing tert-butanol (as well as sec-butanol).

For the case of n-butanol, the effect of increasing the sample alcohol content on the SANS data is displayed in figure 3. One observes that the simple polydisperse core–shell model successfully fits all of the n-butanol data sets. A polydisperse core–shell model that makes use of a diffuse, rather than a step, density profile for the interface also fits the data successfully [25]. The effective values of the droplet size and density parameters obtained from the two models turn out to be essentially identical.

The effect of alcohol content on the data for tert-butanol is shown in figure 4. For α-values below $\approx$2–3, the fits to the data sets using the simple polydisperse core–shell model are of reasonable quality, however the inclusion of shape fluctuations in the model leads to a marked improvement in the fits (see figures 4(a) and (b)). For the case of $\alpha = 1.8$, the effect of incorporating shape fluctuations is illustrated in figure 5. The improvement in fit is much less successful for higher values of α (see figures 4(c) and (d)), primarily due to the appearance of spurious low-amplitude oscillations appearing at intermediate and high Q when incorporating fluctuations. In all probability, the oscillations originate from the fact that corrections due to

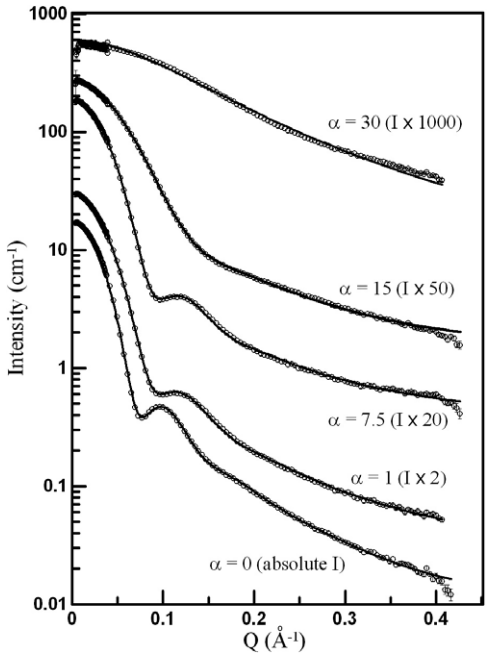

Figure 3. SANS data (with shell contrast) for microemulsions containing various molar ratios, α, of n-butanol-to-AOT. The data sets are shifted vertically for purposes of visibility. The solid lines are the best fits based on the simple polydisperse core–shell model.

shape fluctuations are based on a Taylor expansion [22], and hence become questionable above about $QR_o|u_2|_{rms} \sim 1$. Based on the parameters extracted from the independent NSE dynamics (refer to table 2), the maximum Q for which the model is robust decreases with increasing α, from $Q_{max} \approx 0.31$ for $\alpha = 1$ to $Q_{max} \approx 0.16$ for $\alpha = 7.5$. It should also be noted that unique fitting parameters could not be obtained for the $\alpha = 30$ microemulsion.

Figure 6 shows the influence of tert-butanol content on the Q-dependence of the effective diffusion coefficient from the NSE experiments. As α increases, the peak systematically broadens, increases in height, and shifts to higher Q, which are trends that are all indicative of increasing $l = 2$ shape fluctuations and increasing flexibility of the interface. The solid curves are the best fits based on the NSE fluctuating droplet model. For comparison, figure 6(b) also displays the data and best fit for the sole n-butanol sample measured by NSE ($\alpha = 1.0$). In this case, both alcohols yield similar values of the fitting parameters.

Table 1 lists the various structural parameters of the droplet, as determined by SANS, for the various alcohol contents and types. It is worth noting that the parameter values for the sec-butanol case always fall between the corresponding values for the other two structures of butyl alcohol. Table 2 is a listing of the various NSE parameters, and also compares the NSE shape fluctuation parameters, $|u_2|_{rms}$ and κ, to the values obtained from SANS.

Figure 7 shows that the droplet size tends to decrease with increasing α, and that the overall trend is similar for the three different alcohol structures. This observation is consistent with the expectation that most alcohol molecules reside near the core–shell interface, with the effect being to decrease the volume-to-surface ratio, and hence decrease the radius of the droplets.

The droplet size fluctuations, i.e. the polydispersities, on the other hand, increase with α once the alcohol content exceeds a certain value, beginning at a base value of $p \approx 0.20$–0.22

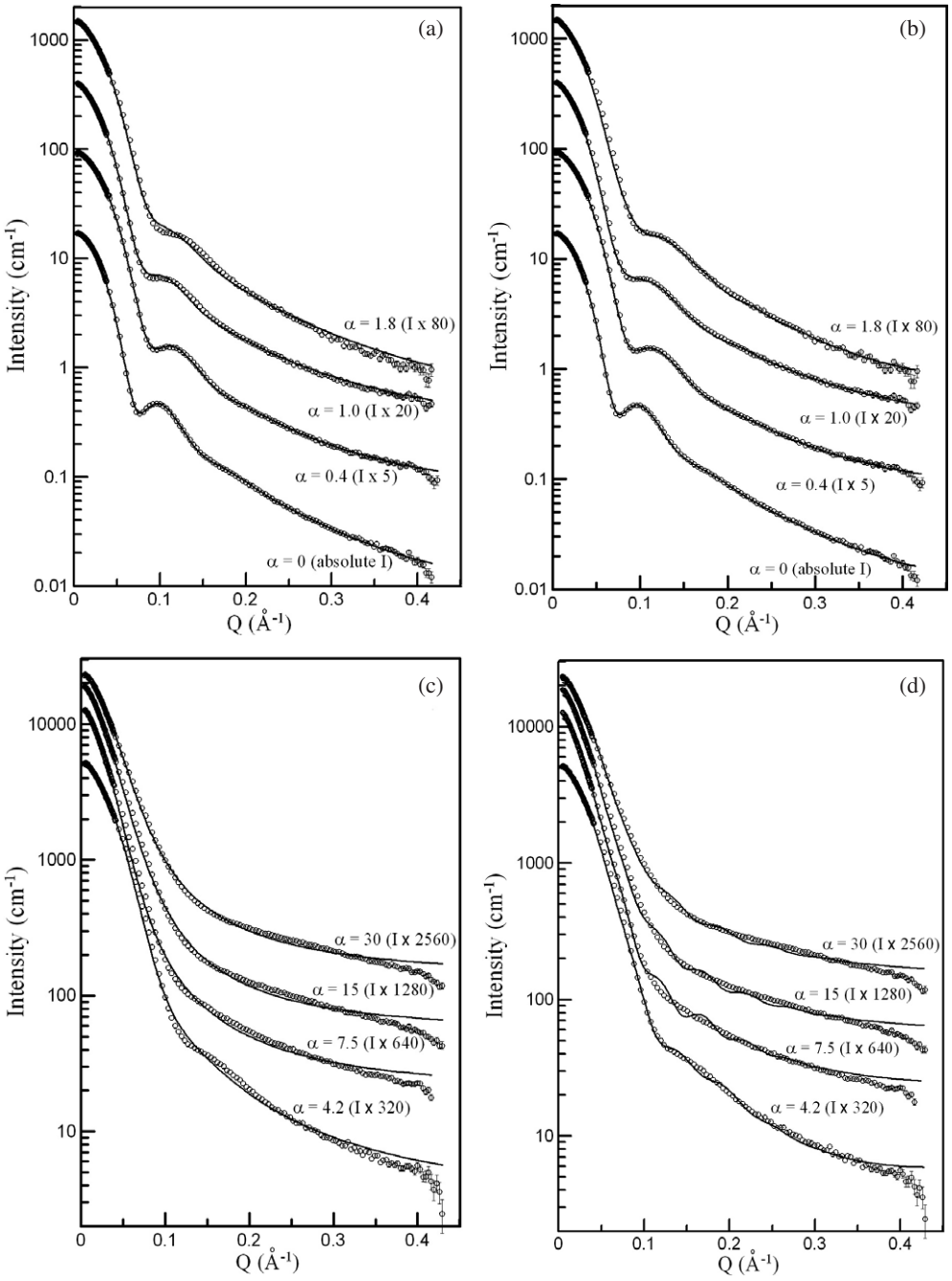

Figure 4. SANS data (with shell contrast) for microemulsions containing various molar ratios, α, of tert-butanol-to-AOT. The data sets are shifted vertically for purposes of visibility. The solid lines are the best fits based on two different models: (a) $\alpha = 0$–1.8, fitted to a simple polydisperse core–shell model; (b) $\alpha = 0$–1.8, fitted to a polydisperse core–shell with shape fluctuations; (c) $\alpha = 4.2$–30, fitted to a simple polydisperse core–shell model; (d) $\alpha = 4.2$–30, fitted to a polydisperse core–shell with shape fluctuations. For the case of $\alpha = 30$ in (c) and (d), the quality of the fits displayed could be obtained using a wide range of fitting-parameter sets, i.e. unique fitting parameters could not be extracted.

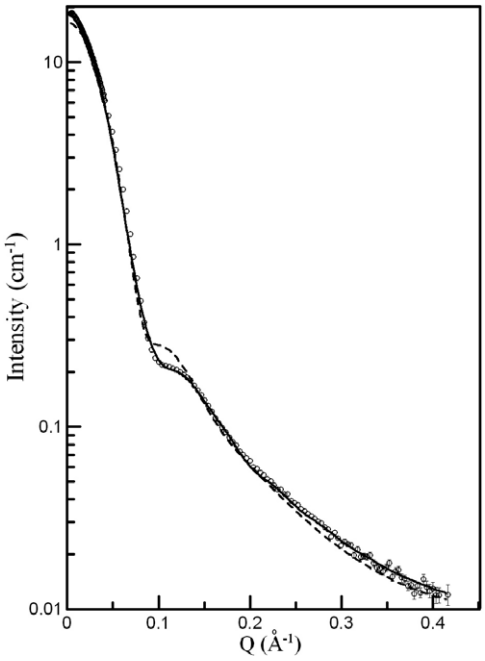

Figure 5. Effect of incorporating shape fluctuations in the SANS model for the microemulsion containing a tert-butanol-to-AOT ratio of $\alpha = 1.8$. The solid curve is the best fit based on the polydisperse core–shell model incorporating shape fluctuations. The dashed curve is calculated using the same fitting parameters as for the solid curve, except for the bending modulus, which is set to $\kappa \to \infty$ (and hence the fluctuation amplitudes, $|u_l|_{\rm rms}$, are forced to vanish).

Table 1. Droplet structural parameters determined from SANS for different values of the alcohol-to-AOT molar ratio, α. Data from samples containing n-butyl alcohol were fitted with the polydisperse core–shell model assuming no shape fluctuations, whereas samples containing tert-butyl alcohol (and also sec-butyl alcohol) were fitted with the model incorporating shape fluctuations. A dash indicates that no sample was available for that composition. (The parameter $f_{\rm BA}$ represents the fraction of the droplet core volume composed of alcohol, computed from (12).)

	$\bar{R}_{\rm c}$ (Å)		δ (Å)		p		$f_{\rm BA}$	
α	n-BA	t-BA	n-BA	t-BA	n-BA	t-BA	n-BA	t-BA
0	35.9 ± 1.4	35.9 ± 1.4	9.9 ± 0.4	9.9 ± 0.4	0.20 ± 0.01	0.20 ± 0.01	0	0
0.4	—	31.7 ± 1.3	—	9.4 ± 0.4	—	0.20 ± 0.01	—	0.11 ± 0.03
1.0	30.4 ± 1.2	35.0 ± 1.4	7.1 ± 0.3	8.9 ± 0.4	0.22 ± 0.01	0.21 ± 0.01	0.06 ± 0.03	0.05 ± 0.03
1.8	—	29.6 ± 1.2	—	11.8 ± 0.5	—	0.26 ± 0.01	—	0.10 ± 0.03
4.2	—	18.9 ± 0.8	—	16.5 ± 0.7	—	0.43 ± 0.02	—	0.16 ± 0.03
7.5	31.4 ± 1.3	20.9 ± 0.8	5.2 ± 0.2	14.3 ± 0.6	0.21 ± 0.01	0.54 ± 0.02	0.05 ± 0.03	0.13 ± 0.03
	s-BA: (24.7 ± 1.0)		(7.2 ± 0.6)		(0.38 ± 0.02)		(0.08 ± 0.03)	
15	15.3 ± 0.6	18.3 ± 0.7	6.4 ± 0.3	10.5 ± 0.4	0.39 ± 0.02	0.66 ± 0.03	0.04 ± 0.03	0.11 ± 0.03

at low α. In the case of the n-butanol microemulsions, the increase is not apparent until α surpasses a value of 7.5, whereas, for the tert-butanol case, the increase is apparent and quite large once α gets to above a value of only $\approx$1. In the n-butanol case, the values of p and the overall trend are in line with polydispersities previously reported for microemulsions of similar composition [13]. The $l = 2$ shape fluctuation parameters are more difficult to

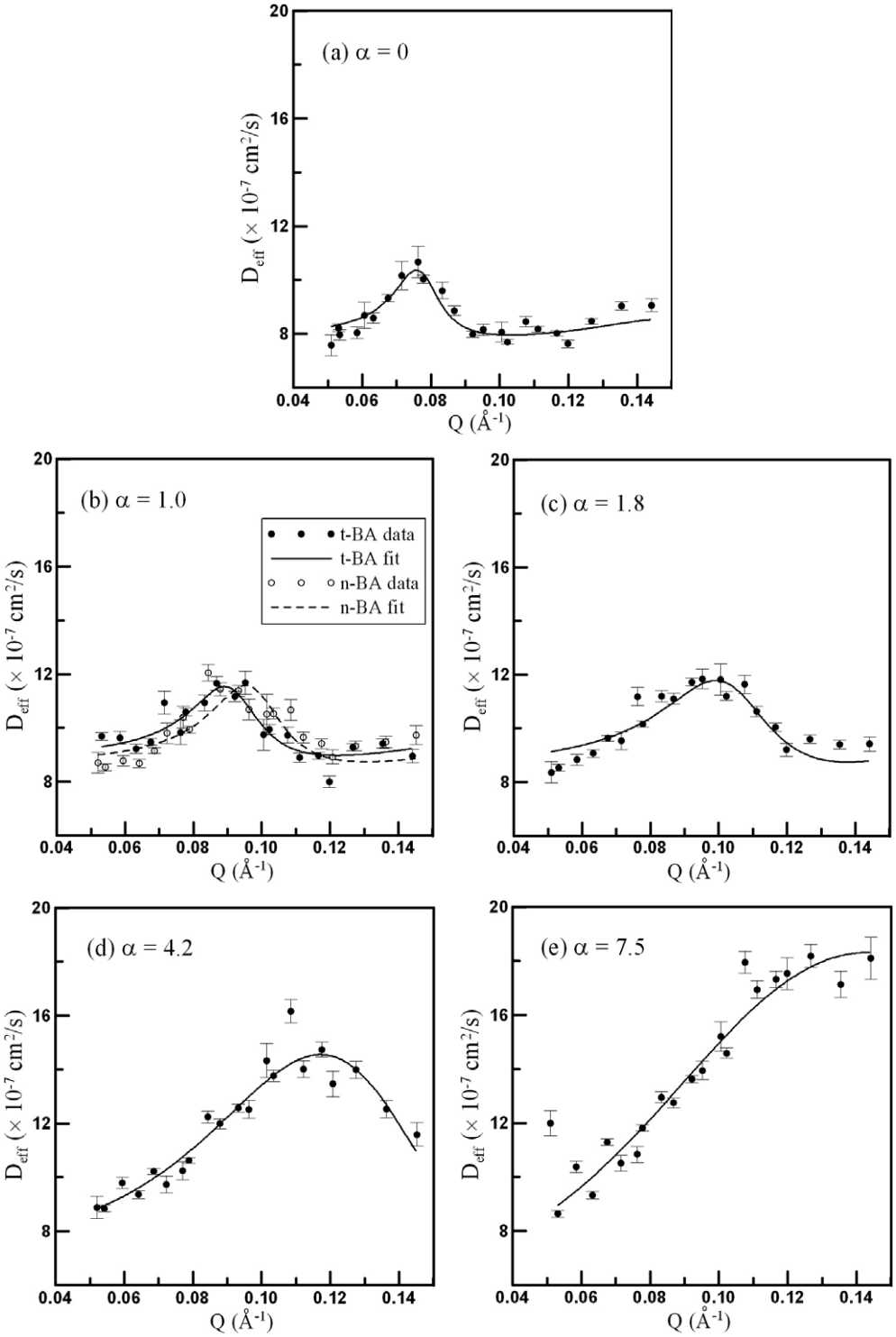

Figure 6. Q-dependence of the effective diffusion coefficient extracted from NSE data for various tert-butanol-to-AOT ratios, α. The curves displayed are the best fits to the data. The data and best fit for the $\alpha = 1$ microemulsion containing n-butyl alcohol are also shown in (b).

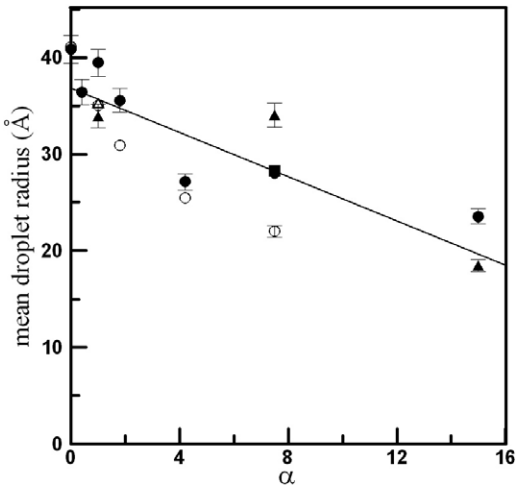

Figure 7. Mean droplet radius as a function of the alcohol-to-AOT ratio. Solid circles (from SANS) and open circles (from NSE) are for microemulsions containing tert-butanol. Solid triangles (from SANS) and open triangle at $\alpha = 1$ (from NSE) are for n-butanol microemulsions. The solid square at $\alpha = 7.5$ (from SANS) is for a sample containing sec-butanol. The sizes from SANS correspond to $\bar{R}_c + \delta/2$, whereas the NSE size is simply the radius R_o. (The line shown is just to indicate the overall trend.)

Table 2. Droplet parameters determined from NSE data for samples containing tert-butyl alcohol. For the shape fluctuation parameters, $|u_2|_{rms}$ and κ/k_BT, the values obtained from NSE are compared to the SANS results based on the model incorporating shape fluctuations. Values in parentheses are for samples containing n-butyl alcohol, whereas values in square brackets correspond to the case of sec-butyl alcohol. An 'x' means that the incorporation of shape fluctuations was unnecessary for successful fitting of the SANS data. A dash indicates that the particular sample was unavailable for the NSE experiments.

		D_{tr} (10^{-7}	λ_2	$\lvert u_2\rvert_{rms}$		κ/k_BT	
α	R_o (Å)	cm^2 s^{-1})	(10^7 Hz)	NSE	SANS	NSE	SANS
0	41.1 ± 0.4	8.19 ± 0.05	1.25 ± 0.02	0.09 ± 0.01	x	0.23 ± 0.01	x
0.4	—	—	—	—	0.19 ± 0.01	—	1.30 ± 0.05
1.0	35.0 ± 0.3	9.48 ± 0.06	1.73 ± 0.16	0.09 ± 0.01	0.27 ± 0.01	0.20 ± 0.02	0.72 ± 0.03
	(35.3 ± 0.2)	(9.28 ± 0.07)	(2.25 ± 0.18)	(0.08 ± 0.01)	(x)	(0.24 ± 0.02)	(x)
1.8	30.9 ± 0.2	8.95 ± 0.09	2.90 ± 0.14	0.15 ± 0.01	0.35 ± 0.01	0.16 ± 0.01	0.44 ± 0.02
4.2	25.5 ± 0.2	8.86 ± 0.12	8.30 ± 0.28	0.21 ± 0.01	0.57 ± 0.02	0.14 ± 0.01	0.16 ± 0.01
7.5	22.0 ± 0.6	7.82 ± 0.14	19.3 ± 1.2	0.27 ± 0.02	0.61 ± 0.02	0.18 ± 0.01	0.14 ± 0.01
					$[0.46 \pm 0.01]$		$[0.24 \pm 0.01]$
					(x)		(x)
15	—	—	—	—	0.45 ± 0.02	—	0.22 ± 0.01
					(x)		(x)

understand. However, if one focuses separately on either the NSE results or the SANS results for the tert-butanol microemulsions, the trend is rather clear: the fluctuation amplitudes, $|u_2|_{rms}$, increase and the elastic bending moduli, κ, exhibit an overall decrease as the alcohol content is raised. However, it is obvious that there is no agreement (except for κ at high α-values) between the actual magnitudes of the parameters from the two types of measurements. Since NSE is a more direct probe of shape fluctuation dynamics, more credence is placed on the

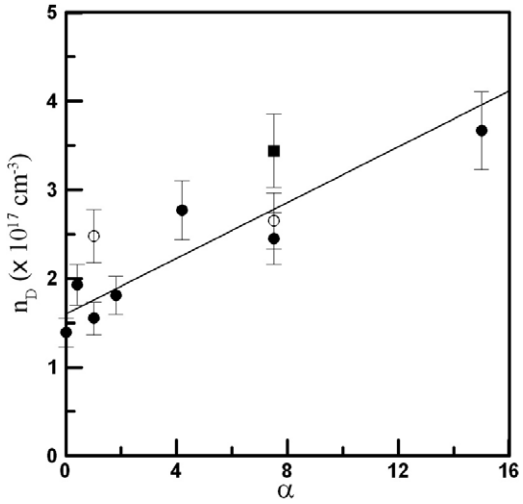

Figure 8. Number density of droplets as a function of alcohol-to-AOT ratio from fitted SANS parameters. Solid circles, open circles, and the solid square correspond to microemulsions containing tert-butanol, n-butanol, and sec-butanol, respectively. (The line shown is just to indicate the overall trend.)

NSE values. The tert-butanol NSE values determined for $|u_2|_{\rm rms}$ are quite similar to those quoted by Farago *et al* and Mihailescu *et al* [13, 26], whereas our κ-values are an order of magnitude lower. On the other hand, our values for κ are consistent with typical results from Kawabata *et al* [10], however our values for $|u_2|_{\rm rms}$ are much lower. As has been pointed out [10–12], SANS and NSE will yield the correct trend for the shape fluctuation parameters; however, the actual numerical values depend quite sensitively on the precise fitting procedures and models employed. It should be noted that for $\alpha = 1$, the only composition measured by NSE for both n-butanol and tert-butanol, little difference is found in the shape fluctuations. However, as emphasized previously, the substantial increases in polydispersity do not yet appear at this alcohol content either, so any definitive statement comparing the trends in $|u_2|_{\rm rms}$ and κ for the two alcohol types would not be justified.

The droplet number density in the microemulsion is $n_{\rm D} = 3\phi/4\pi\langle(R_{\rm c}+\delta)^3\rangle$, where, for a Schultz polydispersity,

$$\left\langle (R_{\rm c}+\delta)^3 \right\rangle = \bar{R}_{\rm c}^3 \left[\left(1+p^2\right)\left(1+2p^2+\frac{3\delta}{\bar{R}_{\rm c}}\right) + 3\left(\frac{\delta}{\bar{R}_{\rm c}}\right)^2 \right]. \tag{11}$$

Since the droplet size tends to shrink with the addition of alcohol, and the total volume of droplets ϕ remains fixed at 6%, the number of droplets per unit volume must be an increasing function of α, as illustrated in figure 8.

The α-dependence of the fitted scattering-length densities of the droplet core and shell are shown in figure 9. We were unable to successfully fit SANS data for the four-component microemulsions ($\alpha \neq 0$) by fixing the scattering-length density of the core to that of pure D_2O. We hypothesize that a small fraction of butyl alcohol ($\rho_{\rm BA} = -0.33 \times 10^{-6}$ Å^{-2}) in the droplet actually resides within the core region, causing the scattering-length density of the core to drop below the pure D_2O value. Another possibility, of course, is that hydrogen–deuterium exchange takes place between alcohol in the shell and D_2O in the core. However, if this were the case, one would expect a systematic drop in $\rho_{\rm c}$ with increasing α (the maximum possible exchange

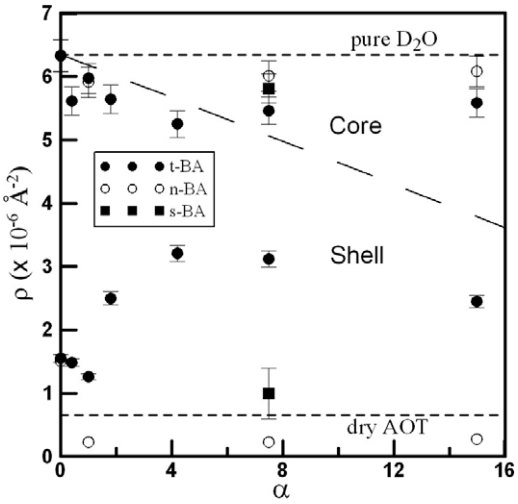

Figure 9. Scattering-length densities, ρ_c and ρ_s, of the droplet core and shell from SANS data as a function of alcohol-to-surfactant ratio for the various butyl alcohol structures. For reference, the scattering-length densities of pure D_2O (6.36×10^{-6} Å^{-2}) and dry AOT (0.63×10^{-6} Å^{-2}) are displayed as well. The tilted dashed line corresponds to the calculated scattering-length density of the core, assuming the maximum possible hydrogen–deuterium exchange between alcohol in the shell and D_2O in the core—this would be the case if 100% of OH-bonded hydrogen in the alcohol undergoes exchange.

effect, where all OH-bonded hydrogen in the alcohol undergoes exchange [27], is indicated by the tilted dashed line in figure 9). Such a trend is not observed, so we conclude that exchange is minimal, and alcohol penetrates into the core. Letting f_{BA} denote the fraction of core volume composed of alcohol, we can write $\rho_c = \rho_{D_2O}(1 - f_{BA}) + \rho_{BA} f_{BA}$, or

$$f_{BA} = \frac{\rho_c - \rho_{D_2O}}{\rho_{BA} - \rho_{D_2O}}. \tag{12}$$

The resulting values of f_{BA} are listed in table 1 showing that, of the three alcohols, tert-butanol has the highest propensity for penetration into the water core. In addition, the highly elevated values of ρ_s for the tert-butanol microemulsions indicates substantial penetration of D_2O into the shell as well. Apparently, the tert-butanol cosurfactant causes the interface between core and shell to become less distinct.

One can calculate an effective surfactant (AOT) head-area at the core–shell interface from

$$a_{eff} = 4\pi \left\langle R_c^2 \right\rangle \frac{n_D}{n_{AOT}}, \tag{13}$$

where n_{AOT}, the surfactant number density, is easily computed from the sample composition. The resulting values are plotted for the different alcohol structures, as a function of alcohol content, in figure 10. If a^o_{eff} is the effective surfactant head-area in the absence of any alcohol, we can define a cosurfactant 'spreading parameter', s, through the relation

$$a_{eff} = a^o_{eff}\,(1 + s\alpha)\,. \tag{14}$$

Clearly, n-butanol ($s = 0.24$) has a much larger spreading effect on the area per surfactant molecule than does tert-butanol ($s = 0.10$), with sec-butanol having an influence somewhere in between. The lower s-value for tert-butanol is consistent with the enhanced penetration of this isomer into the water core, making fewer of the molecules available to produce spreading at the core–shell interface.

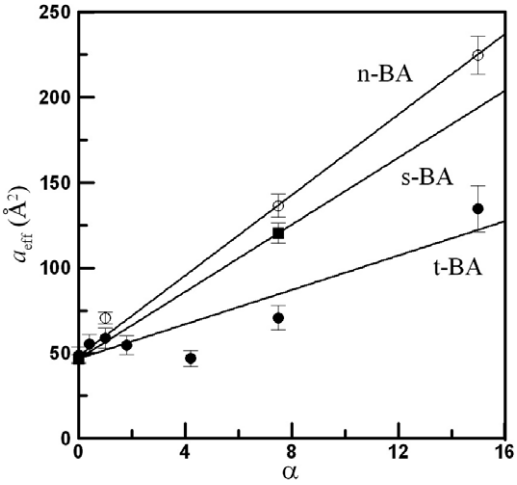

Figure 10. Effective AOT head-area as a function of alcohol-to-AOT ratio for microemulsions containing tert-butanol (solid circles), n-butanol (open circles), and sec-butanol (solid square). In the absence of alcohol ($\alpha = 0$), the value of the effective head-area agrees reasonably well with the previously published value [19] of $\sim$60 Å^2. The displayed best-fit straight line to each set leads to a different value of s, the 'spreading parameter,' for the three different alcohol structures.

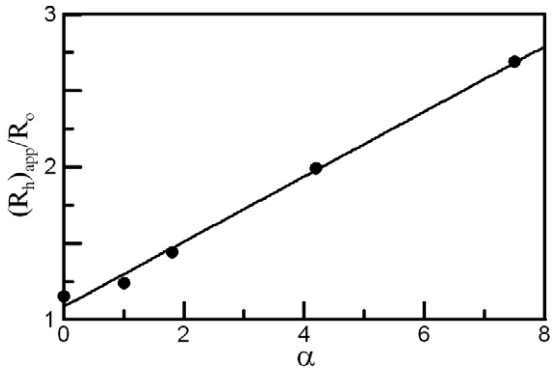

Figure 11. Ratio of the apparent hydrodynamic radius, $(R_h)_{app}$, to the mean droplet radius, R_o, as a function of tert-butanol content, α.

The translational diffusion coefficients in table 2 essentially correspond to the $Q \rightarrow 0$ extrapolated values of the solid curves in figure 6. We found that the tabulated values of D_{tr} are comparable to values that we obtained from dynamic light scattering measurements on the same set of samples. The apparent hydrodynamic radii, $(R_h)_{app}$, based on applying the Stokes–Einstein relation to the listed values of D_{tr} are always larger than the corresponding fitted values of the actual droplet radius R_o. The ratio $(R_h)_{app}/R_o$ is found to increase linearly with α, as shown in figure 11. If one neglects hydrodynamic interactions, then, for spherical droplets, $(R_h)_{app}/R_o \approx S(0)$ (i.e. the interparticle structure factor in the $Q \rightarrow 0$ limit). Values greater than one signify the presence of sizeable attractive droplet–droplet interactions. The rise in the attraction with increasing α is consistent with cloud-point measurements that we have performed on the tert-butanol microemulsions. In particular, the three-component system exhibits a lower critical solution temperature point which lies above room temperature.

The effect of incorporating tert-butanol, and increasing the value of α, is to shift the phase-separation boundary to lower temperatures (i.e. closer and closer to the sample temperature of 23 °C), hence increasing attractions between droplets and driving a phase separation.

5. Summary

The partitioning of added butyl alcohol cosurfactants to the microemulsion droplets causes a decrease in droplet size, and enhances size and shape fluctuations. The increase in polydispersity is much larger in the tert-butanol case. The influence on surface 'spreading' at the core–shell interface is lowest in the case of tert-butanol because of the enhanced penetration of this alcohol into the water core. The addition of tert-butanol leads to increased interdroplet interactions, driving the system towards phase separation.

Acknowledgments

The authors would like to thank the staff of the Center for High Resolution Neutron Scattering for access to and assistance with the NG3 30 m SANS instrument and the neutron spin-echo spectrometer at the NIST Center for Neutron Research. We are also grateful to Professor G M Thurston for assistance with SANS data collection and helpful discussions, and to Mr M D Gawryla and Mr G M Wright for sample preparation and other assistance. This research was partially supported by an award from Research Corporation and this work utilized facilities supported in part by the National Science Foundation under Agreement No. DMR-0454672. Manufacturers are identified in order to provide complete identification of experimental conditions, and such identification is not intended as a recommendation by the University of Maryland or NIST.

References

[1] Huang J S, Kotlarchyk M and Chen S H 1990 Structure and properties of three-component microemulsions near the critical point *Micellar Solutions and Microemulsions Structure Dynamics and Statistical Thermodynamics* ed S H Chen and R Rajagopalan (New York: Springer) pp 227–49
[2] Chen S H, Lin T L and Huang J S 1987 Structure and phase transitions of a three-component microemulsion system: AOT/water/alkane *Physics of Complex and Supermoleclar Fluids* ed S A Safran and N A Clark (New York: Wiley) pp 285–313
[3] Kotlarchyk M, Sheu E Y and Capel M 1992 *Phys. Rev.* A **46** 928
[4] Kotlarchyk M, Chen S H, Huang J S and Kim M W 1984 *Phys. Rev.* A **29** 2054
[5] Safran S A 1983 *J. Chem. Phys.* **78** 2073
[6] Mezei F 2003 Fundamentals of neutron spin echo spectroscopy *Neutron Spin Echo Spectroscopy* ed F Mezei, C Pappas and T Gutberlet (Berlin: Springer) pp 5–14
[7] Farago B 1996 *Physica* B **226** 51
[8] Farago B, Monkenbusch M, Goecking K D, Richter D and Huang J S 1995 *Physica* B **213/214** 712
[9] Huang J S, Milner S T, Farago B and Richter D 1987 *Phys. Rev. Lett.* **59** 2600
[10] Kawabata Y, Nagao M, Seto H, Komura S, Takeda T, Schwahn D, Yamada N L and Nobutou H 2004 *Phys. Rev. Lett.* **92** 056103
[11] Hellweg T and Langevin D 1999 *Physica* A **264** 370
[12] Hellweg T and Langevin D 1998 *Phys. Rev.* E **57** 6825
[13] Farago B, Richter D, Huang J S, Safran S A and Milner S T 1990 *Phys. Rev. Lett.* **65** 3348
[14] Sheu E Y, Chen S H, Huang J S and Sung J C 1989 *Phys. Rev.* A **39** 5867
[15] http://www.ncnr.nist.gov/
[16] http://www.ncnr.nist.gov/programs/sans/data/red_anal.html

[17] Rosov N, Rathgeber S and Monkenbusch M 2000 Neutron spin echo spectroscopy at the NIST Center for Neutron Research *Scattering from Polymers: Characterization by X-Rays, Neutrons and Light* (*ACS Symp. Series* vol 739) ed P Cebe, B S Hsaio and D J Lohse (Washington, DC: American Chemical Society) pp 103–16
[18] http://www.ncnr.nist.gov/dave
[19] Kotlarchyk M, Stephens R B and Huang J S 1988 *J. Phys. Chem.* **92** 1533
[20] Kotlarchyk M and Chen S H 1983 *J. Chem. Phys.* **79** 2461
[21] Hellweg T, Gradzielski M, Farago B, Langevin D and Safran S 2003 *Colloids Surf.* A **221** 257
[22] Farago B and Gradzielski M 2001 *J. Chem. Phys.* **114** 10105
[23] Milner S T and Safran S A 1987 *Phys. Rev.* A **36** 4371
[24] Kawabata Y, Seto H, Nagao M and Takeda T 2002 *J. Neutron Res.* **10** 131
[25] Gradzielski M, Langevin D, Magid L and Strey R 1995 *J. Phys. Chem.* **99** 13232
[26] Mihailescu M, Monkenbusch M, Endo H, Allgaier J, Gompper G, Stellbrink J and Richter D 2001 *J. Chem. Phys.* **115** 9563
[27] Jacrot B 1976 *Rep. Prog. Phys.* **39** 911